



Chaotic discrete breathers in bcc lattice

I.D. Kolesnikov^a, S.A. Shcherbinin^{b,c}, Yu.V. Bebikhov^d, E.A. Korznikova^{d,e,f}, I.A. Shepelev^g,
A.A. Kudreyko^h, S.V. Dmitriev^{i,j,*}

^a Saratov State University, Astrakhanskaya St. 83, Saratov 410012, Russia

^b Peter the Great St. Petersburg Polytechnic University, Polytechnicheskaya St. 29, 195251, St. Petersburg, Russia

^c Institute for Problems in Mechanical Engineering, Russian Academy of Sciences, V. O., Bolshoj Ave., 61, 199178, St. Petersburg, Russia

^d Polytechnic Institute (Branch) in Mirny, North-Eastern Federal University, Tikhonova St. 5/1, 678170 Mirny, Sakha Republic (Yakutia), Russia

^e Institute for Metals Superplasticity Problems, Russian Academy of Sciences, Khalturin St. 39, Ufa 450001, Russia

^f Department of Technological Machines and Equipment, Ufa State Petroleum Technological University, Kosmonavtov St. 1, 450064 Ufa, Russia

^g Almeteyevsk State Petroleum Institute, Lenin St., 2, Almeteyevsk 423462, Russia

^h Bashkir State Medical University, Lenin St. 3, 450008 Ufa, Russia

ⁱ Institute of Molecule and Crystal Physics, UFRС of Russian Academy of Sciences, Oktyabrya Ave. 151, Ufa 450075, Russia

^j Department of Equipment and Technologies of Welding and Control, Ufa State Petroleum Technological University, Kosmonavtov St. 1, 450064 Ufa, Russia

ARTICLE INFO

Keywords:

Bcc lattice
Nonlinear dynamics
Modulational instability
Discrete breather

ABSTRACT

It is well known that a modulationally unstable short-wavelength delocalized nonlinear vibrational mode (DNVM) can create chaotic discrete breathers (DBs) in a nonlinear lattice. A necessary condition for this is that the DNVM must have a frequency outside the phonon spectrum of the lattice. This phenomenon has been repeatedly analyzed for one- and two-dimensional lattices, and here it is studied for a bcc lattice with β -Fermi–Pasta–Ulam–Tsingou potential. Using the group-theoretical approach developed by Chechin and Sakhenko, four DNVMs are found with a wave vector at the boundary of the first Brillouin zone and frequencies above the phonon spectrum. It is shown that the development of the modulational instability of all four DNVMs with amplitudes above a certain value leads to the formation of chaotic DBs, which is justified by calculating the energy localization parameter and the maximum particle energy. Chaotic DBs in the three-dimensional bcc lattice radiate their energy faster than in previously studied two-dimensional lattices. The results obtained describe one of the possible mechanisms of energy dissipation by a crystal lattice in a far-from-equilibrium system.

1. Introduction

Pioneer works [1–3] showed that spatial localization of vibrational energy is possible in defect-free nonlinear lattices. Such high-amplitude localized oscillations are called discrete breathers (DBs) or intrinsic localized modes. Many interesting results on DBs, summarized in the reviews [4–6], were obtained for one-dimensional and, more rarely, two-dimensional lattices [7,8]. The desire to elucidate the role of DBs in crystal physics leads to the need to study three-dimensional lattices [9]. Experimental study of discrete breathers in crystals is based on the measurement of vibrational spectra using the methods of Raman scattering, X-ray and neutron scattering [10–13]. In theory, the method of molecular dynamics is actively used, which made it possible to show the existence of discrete breathers in ionic crystals [14–16], covalent crystals [17,18], metals with fcc [19–25], bcc [19,26–28], and hcp [29,30] lattices, in α -uranium [31], in ordered alloys [32,33], on the surface of a crystal [34], as well as in crystals with Morse

potential [35,36], coronene [37], carbon nanotubes [38–41], honeycomb structures [42], graphene [43–46] and graphane [47,48]. The interaction of DBs with defects in the crystal structure [40,49–52] and their influence on the macroscopic properties of crystals [53–57] are studied. The problem of finding DBs in crystals at thermal equilibrium has been addressed [16,35,58].

In 1990, Burlakov, Kiselev and Rupasov discovered a very unexpected phenomenon of the spontaneous appearance of DBs in a nonlinear chain as a result of the development of the modulation instability of a vibrational mode with a wave vector at the boundary of the first Brillouin zone [59]; such DBs were called chaotic. This phenomenon, sometimes related to the anti-Fermi–Pasta–Ulam–Tsingou (FPUT) problem [60], has been comprehensively studied for one-dimensional [59–66] and two-dimensional lattices [8,60,67,68], but for three-dimensional systems, to date, there is a very limited number of works [20]. Daumont, Dauxois, and Peyrard have shown how the discreteness drastically modifies the modulational instability condition and also noted that it is the first step to energy localization

* Corresponding author at: Institute of Molecule and Crystal Physics, UFRС of Russian Academy of Sciences, Oktyabrya Ave. 151, Ufa 450075, Russia.
E-mail address: dmitriev.sergey.v@gmail.com (S.V. Dmitriev).

in the nonlinear chain [61]. Yoshimura has studied the modulational instability of the zone boundary mode in nonlinear chains with generic polynomial potentials and presented an exact expression of the instability growth rate [62]. Kosevich and Lepri have studied modulational instability and energy localization in an anharmonic chain within a continuum theory and described the initial localization stage as a gas of envelope solitons [63].

A necessary condition for the creation of chaotic DBs by an unstable zone-boundary mode is that its frequency must lie outside the phonon band of the lattice. In this case, the energy of the zone-boundary mode cannot be directly transferred to extended phonons, and the development of instability leads to energy localization on chaotic DBs.

In view of this, a consistent study of chaotic DBs arising as a result of the modulation instability of short-wavelength modes should begin with a search for modes that have frequencies outside the phonon spectrum. This problem can be solved on the basis of the group-theoretical approach developed by Chechin and Sakhnenko [69], which derives such modes from the symmetry analysis of the considered lattice. Using this approach, it was shown that for lattices of higher dimensions, the existence of more than one zone-boundary mode with a frequency outside the phonon band is possible. For example, there are three such modes in a triangular lattice [56,70], two in a square lattice [71,72], three in an fcc lattice [73] and four in a bcc lattice [74].

An introduction to the group-theoretical approach of Chechin and Sakhnenko can be found in the appendices to Ref. [70]. This approach is aimed at finding exact oscillatory solutions to the equations of motion of a nonlinear discrete system considering only the symmetry of the system and, therefore, such solutions exist independently of the type of interatomic interactions and for an arbitrary amplitude. Such solutions can be obtained for molecules [75], for infinite lattices [76–78], or for finite size lattices [79]. In the original papers they were called bushes of nonlinear normal modes, but in some studies related to lattices they are called delocalized nonlinear vibrational modes (DNVMs) and the latter term will be used here.

DNVMs can be used to check the accuracy of interatomic potentials for molecular dynamics simulations [80].

It should be said that the study of the nonlinear dynamics of the bcc lattice is of interest, since a number of metals have such a lattice, for example, iron, tungsten, tantalum, molybdenum, niobium, vanadium, chromium, manganese, and barium.

The natural question is how to excite DNVMs in crystals. The successes of recent years in the development of laser technologies have opened up new ways of perturbing the crystal lattice of materials at terahertz frequencies, making it possible to induce forced vibrations of atoms with amplitudes of a few percent of the interatomic distance (see reviews [81–86]). The use of ultrashort laser pulses to perturb crystalline samples on subpicosecond time scales is becoming an increasingly accessible experimental technique. In most condensed matter experiments performed to date, such pulses cause strong athermal excitation of electrons, which relax mainly by electron–electron scattering followed by thermalization by coupling with phonon degrees of freedom. Some DNVMs have frequencies above the phonon spectrum, and their excitation can be expected under the action of a laser pulse with such a frequency. Further evolution of the excited DNVMs can in principle lead to the formation of chaotic DBs.

The role of DBs and DNVMs in far-from-equilibrium states of metals under plastic deformation, irradiation, ion implantation, and laser processing is not fully understood. The present study is a step in this direction.

In the rest of the paper, the FPUT bcc lattice is described in Section 2. The phonon dispersion relation for the lattice is derived in Section 3, DNVMs with frequencies above the phonon band are described in Section 4. In Section 5, the modulational instability of DNVMs and formation of chaotic DBs are studied numerically. The results are summarized in Section 6.

2. FPUT bcc lattice

A three-dimensional bcc β -FPUT lattice with nearest and next-nearest neighbor interactions is considered, see Fig. 1(a). The bcc lattice with the step h is a set of points in the three-dimensional space with radius vectors

$$\xi_{i,j,k} = ie_1 + je_2 + ke_3, \quad (1)$$

where i, j and k are integers and the basis vectors of the lattice are $e_1 = (h, 0, 0)$, $e_2 = (0, h, 0)$ and $e_3 = 1/2(h, h, h)$.

The lattice points are occupied by the particles of mass m , each having three degrees of freedom, the components of the displacement vector $\delta_{i,j,k} = (u_{i,j,k}, v_{i,j,k}, w_{i,j,k})$. Position of the particle i, j, k at time t is given by the radius vector $\mathbf{r}_{i,j,k}(t) = \xi_{i,j,k} + \delta_{i,j,k}(t)$.

Each particle interacts with the eight nearest (n) and six next-nearest (nn) neighbors via the β -FPUT potential

$$\varphi_{n,nn}(r) = \frac{c_{n,nn}}{2}(r - a_{n,nn})^2 + \frac{\beta_{n,nn}}{4}(r - a_{n,nn})^4, \quad (2)$$

where r is the distance between the particles, $a_n = \sqrt{3}h/2$ and $a_{nn} = h$ for the nearest and next-nearest bonds, respectively; c_n and c_{nn} (β_n and β_{nn}) are the coefficients for the harmonic (anharmonic) part of the potential for the nearest and next-nearest bonds, respectively. We take $h = 1$ and $c_n = 1$ by choosing the units of distance and energy, respectively. For simplicity, $c_{nn} = 1$ is set. For the anharmonicity coefficients we set $\beta_n = \beta_{nn} = 10$, then the nonlinearity effects become noticeable for particle displacements of the order of $0.1h$. For the particle mass $m = 1$ is set by defining a unit of time.

Referring to Fig. 1(a), we define the following vectors connecting the nearest and next-nearest neighbors of the i, j, k particle:

$$\begin{aligned} \mathbf{R}_{i,j,k,1} &= \mathbf{r}_{i,j,k-1} - \mathbf{r}_{i,j,k}, \\ \mathbf{R}_{i,j,k,2} &= \mathbf{r}_{i+1,j,k-1} - \mathbf{r}_{i,j,k}, \\ \mathbf{R}_{i,j,k,3} &= \mathbf{r}_{i+1,j+1,k-1} - \mathbf{r}_{i,j,k}, \\ \mathbf{R}_{i,j,k,4} &= \mathbf{r}_{i,j+1,k} - \mathbf{r}_{i,j,k}, \\ \mathbf{R}_{i,j,k,5} &= \mathbf{r}_{i-1,j-1,k+1} - \mathbf{r}_{i,j,k}, \\ \mathbf{R}_{i,j,k,6} &= \mathbf{r}_{i,j-1,k+1} - \mathbf{r}_{i,j,k}, \\ \mathbf{R}_{i,j,k,7} &= \mathbf{r}_{i,j,k+1} - \mathbf{r}_{i,j,k}, \\ \mathbf{R}_{i,j,k,8} &= \mathbf{r}_{i-1,j,k+1} - \mathbf{r}_{i,j,k}, \\ \mathbf{R}_{i,j,k,9} &= \mathbf{r}_{i,j-1,k} - \mathbf{r}_{i,j,k}, \\ \mathbf{R}_{i,j,k,10} &= \mathbf{r}_{i,j+1,k} - \mathbf{r}_{i,j,k}, \\ \mathbf{R}_{i,j,k,11} &= \mathbf{r}_{i-1,j,k} - \mathbf{r}_{i,j,k}, \\ \mathbf{R}_{i,j,k,12} &= \mathbf{r}_{i+1,j,k} - \mathbf{r}_{i,j,k}, \\ \mathbf{R}_{i,j,k,13} &= \mathbf{r}_{i+1,j+1,k-2} - \mathbf{r}_{i,j,k}, \\ \mathbf{R}_{i,j,k,14} &= \mathbf{r}_{i-1,j-1,k+2} - \mathbf{r}_{i,j,k}. \end{aligned} \quad (3)$$

Computational cell includes $I \times J \times K$ particles subject to the periodic boundary conditions, $\mathbf{r}_{i,j,k} = \mathbf{r}_{i+I,j,k} = \mathbf{r}_{i,j+J,k} = \mathbf{r}_{i,j,k+K}$. The Hamiltonian (total energy) of the computational cell is the sum of the kinetic energy of particles and potential energies of the nearest and next-nearest bonds:

$$\begin{aligned} H &= K + P_n + P_{nn} = \sum_{i=1}^I \sum_{j=1}^J \sum_{k=1}^K \frac{m}{2} |\dot{\mathbf{r}}_{i,j,k}|^2 \\ &+ \frac{1}{2} \sum_{i=1}^I \sum_{j=1}^J \sum_{k=1}^K \left(\sum_{s=1}^8 \varphi_n(|\mathbf{R}_{i,j,k,s}|) + \sum_{l=9}^{14} \varphi_{nn}(|\mathbf{R}_{i,j,k,l}|) \right), \end{aligned} \quad (4)$$

where overdot means differentiation with respect to time.

The Hamilton's equations of motion derived from Eq. (4) are

$$m\ddot{u}_{i,j,k} = \sum_{s=1}^8 D_n \mathbf{R}_{i,j,k,s,x} + \sum_{l=9}^{14} D_{nn} \mathbf{R}_{i,j,k,l,x},$$

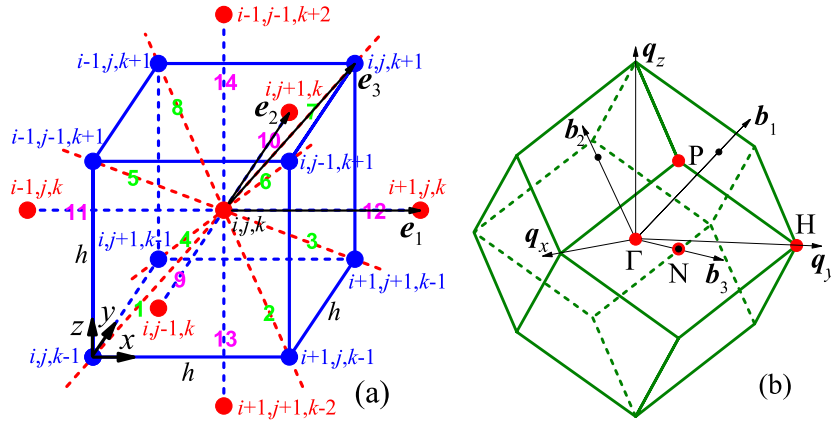


Fig. 1. (a) Cubic translational cell of the bcc lattice with the lattice parameter equal to h . The bcc lattice can be regarded as a union of two simple cubic lattices shifted one with respect to another by the vector $1/2(h, h, h)$. Vectors $e_1 = (h, 0, 0)$, $e_2 = (0, h, 0)$, and $e_3 = 1/2(h, h, h)$ show a non-orthogonal primitive translational cell of the lattice containing single particle. The nearest and next-nearest bonds are taken into account, they are colored red and blue, respectively. Nearest and next-nearest bonds have length $h\sqrt{3}/2$ and h , respectively. (b) The first Brillouin zone of the bcc lattice. (For interpretation of the references to color in this figure legend, the reader is referred to the web version of this article.)

$$m\ddot{v}_{i,j,k} = \sum_{s=1}^8 D_n R_{i,j,k,s,y} + \sum_{l=9}^{14} D_{nn} R_{i,j,k,l,y},$$

$$m\ddot{w}_{i,j,k} = \sum_{s=1}^8 D_n R_{i,j,k,s,z} + \sum_{l=9}^{14} D_{nn} R_{i,j,k,l,z}, \quad (5)$$

where

$$D_n = \frac{\phi'_n(|\mathbf{R}_{i,j,k,s}|)}{|\mathbf{R}_{i,j,k,s}|}, \quad D_{nn} = \frac{\phi'_{nn}(|\mathbf{R}_{i,j,k,l}|)}{|\mathbf{R}_{i,j,k,l}|}. \quad (6)$$

In the Appendix it is shown how the equations of motion Eq. (5) are obtained from the Hamiltonian Eq. (4).

The influence of the computational cell size is studied considering $I = J = K/2 = 10, 20$ and 40 . The total number of particles for these three cases is $2000, 16\,000$ and $128\,000$, respectively.

The equations of motion are integrated numerically employing the symplectic Störmer integrator of order six [87] with the time step of 0.001 time units.

3. Phonon dispersion relation

Assuming that $u_{i,j,k}$, $v_{i,j,k}$, and $w_{i,j,k} \ll h$, we expand the right-hand side of Eq. (5) and discard terms with powers greater than linear, obtaining linearized equations of motion

$$m\ddot{u}_{i,j,k} = c_{nn}(u_{i-1,j,k} - 2u_{i,j,k} + u_{i+1,j,k})$$

$$+ \frac{c_n}{3}(u_{i,j,k-1} - 2u_{i,j,k} + u_{i,j,k+1})$$

$$+ \frac{c_n}{3}(v_{i,j,k-1} - 2v_{i,j,k} + v_{i,j,k+1})$$

$$+ \frac{c_n}{3}(w_{i,j,k-1} - 2w_{i,j,k} + w_{i,j,k+1})$$

$$+ \frac{c_n}{3}(u_{i+1,j,k-1} - 2u_{i,j,k} + u_{i-1,j,k+1})$$

$$- \frac{c_n}{3}(v_{i+1,j,k-1} - 2v_{i,j,k} + v_{i-1,j,k+1})$$

$$- \frac{c_n}{3}(w_{i+1,j,k-1} - 2w_{i,j,k} + w_{i-1,j,k+1})$$

$$+ \frac{c_n}{3}(u_{i+1,j+1,k-1} - 2u_{i,j,k} + u_{i-1,j-1,k+1})$$

$$+ \frac{c_n}{3}(v_{i+1,j+1,k-1} - 2v_{i,j,k} + v_{i-1,j-1,k+1})$$

$$- \frac{c_n}{3}(w_{i+1,j+1,k-1} - 2w_{i,j,k} + w_{i-1,j-1,k+1})$$

$$+ \frac{c_n}{3}(u_{i,j+1,k-1} - 2u_{i,j,k} + u_{i,j-1,k+1})$$

$$- \frac{c_n}{3}(v_{i,j+1,k-1} - 2v_{i,j,k} + v_{i,j-1,k+1})$$

$$+ \frac{c_n}{3}(w_{i,j+1,k-1} - 2w_{i,j,k} + w_{i,j-1,k+1}), \quad (7)$$

$$m\ddot{v}_{i,j,k} = c_{nn}(v_{i,j-1,k} - 2v_{i,j,k} + v_{i,j+1,k})$$

$$+ \frac{c_n}{3}(u_{i,j,k-1} - 2u_{i,j,k} + u_{i,j,k+1})$$

$$+ \frac{c_n}{3}(v_{i,j,k-1} - 2v_{i,j,k} + v_{i,j,k+1})$$

$$+ \frac{c_n}{3}(w_{i,j,k-1} - 2w_{i,j,k} + w_{i,j,k+1})$$

$$- \frac{c_n}{3}(u_{i+1,j,k-1} - 2u_{i,j,k} + u_{i-1,j,k+1})$$

$$+ \frac{c_n}{3}(v_{i+1,j,k-1} - 2v_{i,j,k} + v_{i-1,j,k+1})$$

$$+ \frac{c_n}{3}(w_{i+1,j,k-1} - 2w_{i,j,k} + w_{i-1,j,k+1})$$

$$+ \frac{c_n}{3}(u_{i+1,j+1,k-1} - 2u_{i,j,k} + u_{i-1,j-1,k+1})$$

$$+ \frac{c_n}{3}(v_{i+1,j+1,k-1} - 2v_{i,j,k} + v_{i-1,j-1,k+1})$$

$$- \frac{c_n}{3}(w_{i+1,j+1,k-1} - 2w_{i,j,k} + w_{i-1,j-1,k+1})$$

$$- \frac{c_n}{3}(u_{i,j+1,k-1} - 2u_{i,j,k} + u_{i,j-1,k+1})$$

$$+ \frac{c_n}{3}(v_{i,j+1,k-1} - 2v_{i,j,k} + v_{i,j-1,k+1})$$

$$- \frac{c_n}{3}(w_{i,j+1,k-1} - 2w_{i,j,k} + w_{i,j-1,k+1}), \quad (8)$$

$$m\ddot{w}_{i,j,k} = c_{nn}(w_{i,j,k-1} - 2w_{i,j,k} + w_{i,j,k+1})$$

$$+ \frac{c_n}{3}(u_{i,j,k-1} - 2u_{i,j,k} + u_{i,j,k+1})$$

$$+ \frac{c_n}{3}(v_{i,j,k-1} - 2v_{i,j,k} + v_{i,j,k+1})$$

$$+ \frac{c_n}{3}(w_{i,j,k-1} - 2w_{i,j,k} + w_{i,j,k+1})$$

$$- \frac{c_n}{3}(u_{i+1,j,k-1} - 2u_{i,j,k} + u_{i-1,j,k+1})$$

$$+ \frac{c_n}{3}(v_{i+1,j,k-1} - 2v_{i,j,k} + v_{i-1,j,k+1})$$

$$+ \frac{c_n}{3}(w_{i+1,j,k-1} - 2w_{i,j,k} + w_{i-1,j,k+1})$$

$$- \frac{c_n}{3}(u_{i+1,j+1,k-1} - 2u_{i,j,k} + u_{i-1,j-1,k+1})$$

$$- \frac{c_n}{3}(v_{i+1,j+1,k-1} - 2v_{i,j,k} + v_{i-1,j-1,k+1})$$

$$+ \frac{c_n}{3}(w_{i+1,j+1,k-1} - 2w_{i,j,k} + w_{i-1,j-1,k+1})$$

$$+ \frac{c_n}{3}(u_{i,j+1,k-1} - 2u_{i,j,k} + u_{i,j-1,k+1})$$

$$+ \frac{c_n}{3}(v_{i,j+1,k-1} - 2v_{i,j,k} + v_{i,j-1,k+1})$$

$$\begin{aligned}
& -\frac{c_n}{3}(v_{i,j+1,k-1} - 2v_{i,j,k} + v_{i,j-1,k+1}) \\
& + \frac{c_n}{3}(w_{i,j+1,k-1} - 2w_{i,j,k} + w_{i,j-1,k+1}). \quad (9)
\end{aligned}$$

It is well-known that the linear equations of motion Eqs. (7)–(9) support the solutions of the form

$$\begin{aligned}
u_{i,j,k} &= U \exp[i(qi + sj + pk - \omega t)], \\
v_{i,j,k} &= V \exp[i(qi + sj + pk - \omega t)], \\
w_{i,j,k} &= W \exp[i(qi + sj + pk - \omega t)], \quad (10)
\end{aligned}$$

where i is imaginary unit, q, s, p are the wavenumbers, i, j, k are arbitrary integers, U, V, W are the components of the eigenvector, ω is frequency and t is time. Substituting Eq. (10) into the linear equations of motion Eqs. (7)–(9) one finds

$$\begin{aligned}
(m\omega^2 + P)U + ZV + SW &= 0, \\
ZU + (m\omega^2 + P)V + QW &= 0, \\
SU + QV + (m\omega^2 + P)W &= 0, \quad (11)
\end{aligned}$$

where

$$\begin{aligned}
P &= -\delta - \gamma - \kappa - \eta - \xi, \\
Z &= -\gamma + \kappa - \eta + \xi, \\
S &= -\gamma + \kappa + \eta - \xi, \\
Q &= -\gamma - \kappa + \eta + \xi, \quad (12)
\end{aligned}$$

and

$$\begin{aligned}
\delta &= 4c_{nn} \sin^2 \frac{q}{2}, \quad \gamma = 4\frac{c_n}{3} \sin^2 \frac{p}{2}, \\
\kappa &= 4\frac{c_n}{3} \sin^2 \frac{q-p}{2}, \quad \eta = 4\frac{c_n}{3} \sin^2 \frac{q+s-p}{2}, \\
\xi &= 4\frac{c_n}{3} \sin^2 \frac{s-p}{2}. \quad (13)
\end{aligned}$$

A homogeneous system of linear equations Eq. (11) in U, V , and W has a non-zero solution if its determinant is equal to zero. This condition leads to a cubic equation in ω^2 which defines three branches of the dispersion relation,

$$\begin{aligned}
m^3\omega^6 + 3Pm^2\omega^4 + (3P^2 - S^2 - Z^2 - Q^2)m\omega^2 \\
+ 2ZQS + P(P^2 - S^2 - Z^2 - Q^2) = 0. \quad (14)
\end{aligned}$$

For our purposes of finding the maximum phonon frequency, it suffices to analyze the special case of $q = s = p$. Then from Eq. (13) one has $\kappa = \xi = 0$ and $\gamma = \eta$. Eqs. (11) obtain the form

$$\begin{aligned}
(m\omega^2 - \delta - 2\gamma)U - 2\gamma V &= 0, \\
-2\gamma U + (m\omega^2 - \delta - 2\gamma)V &= 0, \\
m\omega^2 &= \delta + 2\gamma. \quad (15)
\end{aligned}$$

The third equation in Eq. (15) defines the dispersion relation for T_2 transverse phonon modes. Two other branches are obtained by equalizing to zero the determinant of the first and second equations of Eq. (15). This leads to the quadratic equation $(m\omega^2 - \delta - 2\gamma)^2 = (2\gamma)^2$ which has the roots

$$m\omega^2 = \delta, \quad m\omega^2 = \delta + 4\gamma. \quad (16)$$

The first dispersion curve in Eq. (16) describes the lowest frequency T_1 transverse phonons and the second — the highest frequency longitudinal phonons.

The highest phonon frequency is achieved on the longitudinal branch at $q = s = p = \pi$:

$$\omega_{\max} = 2\sqrt{\frac{1}{m}\left(\frac{4}{3}c_n + c_{nn}\right)}. \quad (17)$$

For $m = 1, c_n = c_{nn} = 1$ one has $\omega_{\max} = 2\sqrt{7/3} = 3.055$.

The three dispersion curves along the line $q = s = p$ are presented in Fig. 2 for $m = 1, c_n = c_{nn} = 1$.

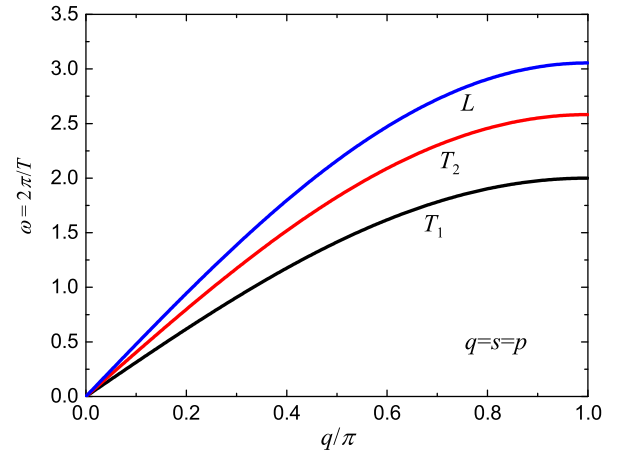


Fig. 2. Dispersion curves of the bcc lattice for the highly symmetrical line of the first Brillouin zone $q = s = p$. The branch of longitudinal phonon vibrations is denoted as L , and the two branches of transverse vibrations are denoted as T_1 and T_2 . Maximal phonon frequency is achieved on the L branch at $q = s = p = \pi$ and is equal to $\omega_{\max} = 2\sqrt{7/3} = 3.055$ for the parameters used in simulations: $m = 1$ and $c_n = c_{nn} = 1$.

4. DNVMs with frequencies above the phonon spectrum

Sixteen one-component DNVMs of bcc lattices have been described in [74]. For the β -FPUT potential with positive β , four of them have frequencies above the phonon spectrum for any amplitude. In this paper, such DNVMs are numbered with Greek numerals from I to IV, see Fig. 3. The presented DNVMs are single-degree-of-freedom vibrational modes.

Initial displacements of particles used for excitation of DNVMs are shown by arrows in the four successive planes parallel to the x, y plane, $z = 0, h/2, h$, and $3h/2$. Cubic translational units of size $2h \times 2h \times 2h$ are shown. Negative and positive displacements along the z axis are shown by the circle with cross and dot, respectively. An empty circle means zero displacement along the z axis. All non-zero displacement vectors have the same length.

In the small-amplitude limit all four DNVMs reduce to the longitudinal phonon modes at the point N of the first Brillouin zone, see Fig. 1(b).

In DNVM III there are particles with zero initial displacement and they remain at rest while initially displaced particles oscillate.

In Fig. 4, the frequency response of DNVMs I–IV is shown in red, blue, black, and green, respectively. The numerically found frequencies are shown by circles, and the lines serve as a guide for the eye. The upper edge of the phonon spectrum is shown as a horizontal dashed line, $\omega_{\max} = 2\sqrt{7/3} = 3.055$.

5. Chaotic discrete breathers

If the DNVM amplitude exceeds the threshold value, it exhibits modulational instability [8,55,64–67,88,89]. The DNVM energy, whose frequency is outside the phonon band, cannot be directly transferred to delocalized phonon waves, so the modulational instability develops by localizing the energy on chaotic DBs.

The following localization parameter can be used to measure the degree of energy localization in the lattice

$$L = N \frac{\sum_{n=1}^N e_n^2}{\left(\sum_{n=1}^N e_n\right)^2}, \quad (18)$$

where N is the number of particles in the system and e_n is the total energy of the n th particle, which is given by

$$e_n = \frac{m}{2} |\dot{\delta}_n|^2 + \frac{1}{2} \sum_{s=1}^8 \varphi_n(|\mathbf{R}_{ns}|) + \frac{1}{2} \sum_{l=9}^{14} \varphi_{nn}(|\mathbf{R}_{nl}|), \quad (19)$$

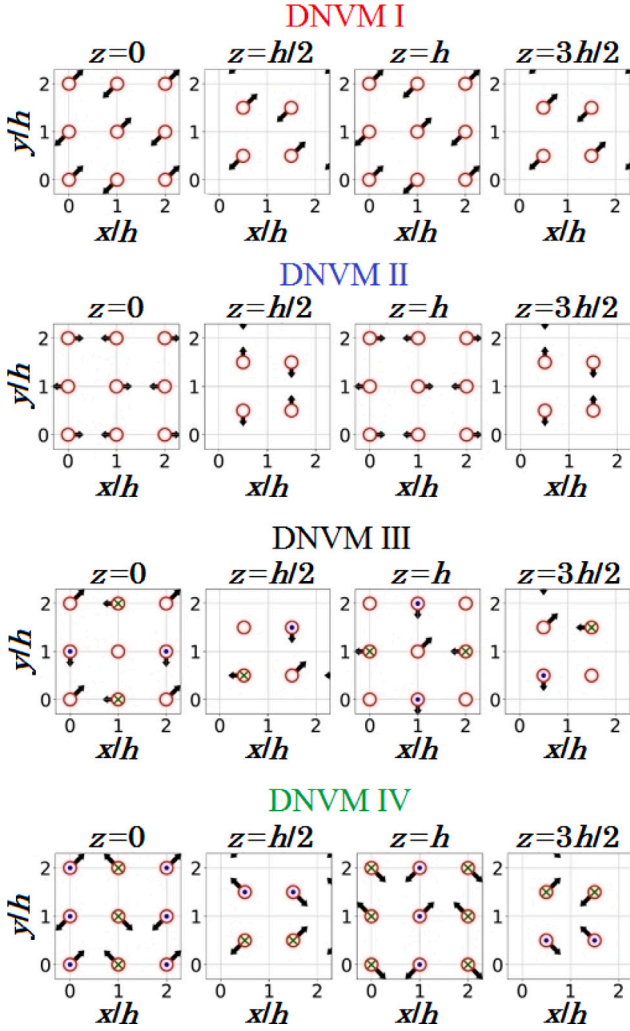


Fig. 3. One-component DNVMs in a bcc lattice with frequencies above the phonon spectrum [74]. Displacements of particles are shown by arrows in four planes: $z = 0$, $z = h/2$, $z = h$, and $z = 3h/2$. Positive (negative) displacements along the z axis are shown by dots (crosses). An empty circle means that the displacement along the z axis is zero.

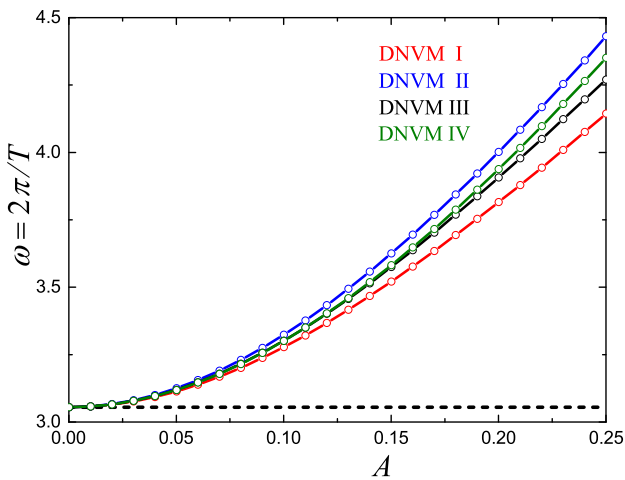


Fig. 4. Frequency as the function of amplitude for DNVMs from I to IV color-coded according to the legend. The highest phonon frequency, $\omega_{\max} = 2\sqrt{7/3} = 3.055$, is shown by the dashed line. (For interpretation of the references to color in this figure legend, the reader is referred to the web version of this article.)

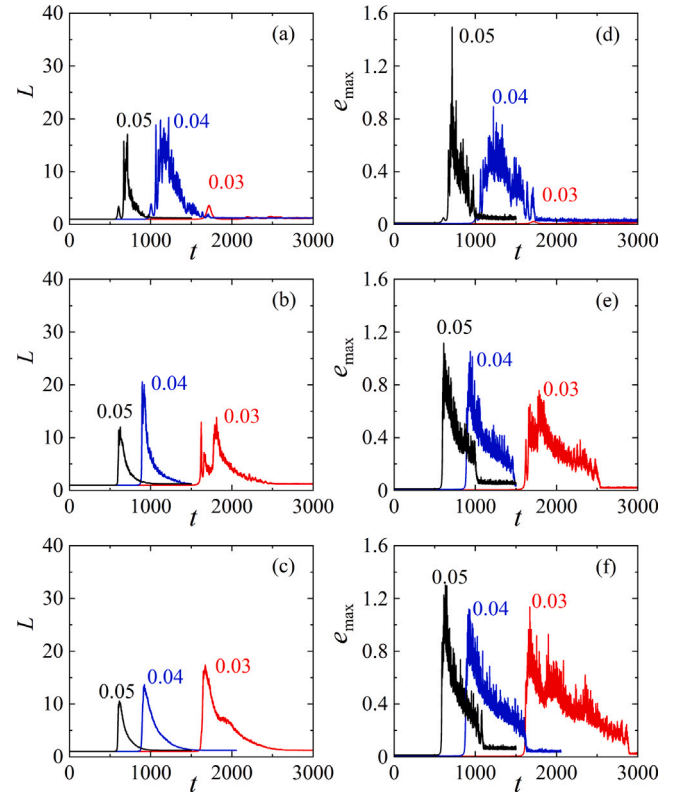


Fig. 5. (a–c) Localization parameter and (d–f) energy of the highest energy particle as the functions of time during the development of the modulational instability of DNVM I. Computational cell size: (a,d) $10 \times 10 \times 20$, (b,e) $20 \times 20 \times 40$, and (c,f) $40 \times 40 \times 80$ particles. Results for three DNVM amplitudes are presented: $A = 0.03$ red line, $A = 0.04$ blue line, and $A = 0.05$ black line. (For interpretation of the references to color in this figure legend, the reader is referred to the web version of this article.)

where the first term is the kinetic energy of the n particle, and the second and third terms sum the halves of the energies of the bonds connecting the n th particle to the nearest and next-nearest particles, respectively. The vectors \mathbf{R}_{ns} and \mathbf{R}_{nl} connect the n th particle to the s th nearest and l th next-nearest particles, respectively.

If the energy of the system belongs to one particle, then $L = N$. If all particles share the energy equally, then $L = 1$.

Figs. 5–8 show numerical results for DNVMs I–IV, respectively. Panels (a–c) show the time course of the localization parameter Eq. (18), and panels (d–f) show the energy of the highest energy particle as a function of time. Three values of the initial DNVM amplitude are analyzed: $A = 0.03$ (red lines), $A = 0.04$ (blue lines) and $A = 0.05$ (black lines). The size of the computational cell also varies. Results for a computation cell including $10 \times 10 \times 20$ particles are shown in (a,d), $20 \times 20 \times 40$ particles in (b,e) and $40 \times 40 \times 80$ particles in (c,f).

The results for all four DNVMs look similar, however some important differences will be identified and explained below.

The localization parameter remains small during the development of the instability and then sharply increases, which is associated with the formation of chaotic DBs in the system. The appearance of DBs is also confirmed by an increase in the energy of the particle with the highest energy synchronously with an increase in the localization parameter. Chaotic DBs gradually radiate their energy in the form of small-amplitude thermal oscillations, which leads to a decrease in L and e_{\max} with time. Finally, the system reaches a state of thermal equilibrium, and L and e_{\max} become small.

If the initial DNVM amplitude A is less than the threshold value, no energy localization occurs, an example of this is the result shown in Fig. 5(a,d) for $A = 0.03$ (red lines) for the smallest computational

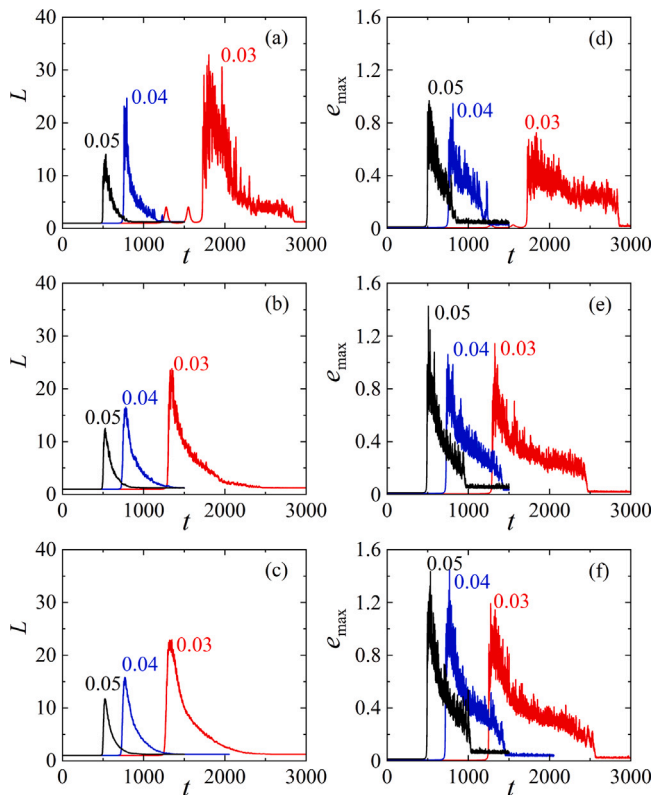


Fig. 6. (a–c) Localization parameter and (d–f) energy of the highest energy particle as the functions of time during the development of the modulational instability of DNVM II. Computational cell size: (a,d) $10 \times 10 \times 20$, (b,e) $20 \times 20 \times 40$, and (c,f) $40 \times 40 \times 80$ particles. Results for three DNVM amplitudes are presented: $A = 0.03$ red line, $A = 0.04$ blue line, and $A = 0.05$ black line. (For interpretation of the references to color in this figure legend, the reader is referred to the web version of this article.)

cell. However, an increase in the size of the computational cell leads to the formation of DBs even at $A = 0.03$, see Fig. 5(b,e) and (c,f). This is due to the fact that in a larger computational cell, the energy for the formation of DBs can be accumulated from a larger volume, and the threshold value of DNVM amplitude becomes smaller.

Only DNVM I with $A = 0.03$ and the smallest computational cell does not produce chaotic DBs, while all other DNVMs produce chaotic DBs under the same conditions. This is because DNVM I has the lowest frequency for the same amplitude, see Fig. 4. A DNVM with a higher frequency interacts less with the phonon band, and the nonlinearity effects are more pronounced.

For a larger initial DNVM amplitude A , the critical exponent of the instability is larger, and the time to a sharp increase in L and e_{\max} is shorter. The computational size effect has little effect on the time to the sharp increase in L and e_{\max} , especially for the initial DNVM amplitudes equal to 0.04 and 0.03.

The maximum localization parameter increases as A decreases, while e_{\max} only slightly decrease as A decreases. It can be concluded that with decreasing A the number of chaotic DBs decreases but their energy is about the same. For smaller A the energy of a chaotic DB is accumulated from a larger volume because the wavelength of the instability wave increases [62,63].

High-energy particles at time t^* , at which the localization parameter reaches its maximum, are shown in Fig. 9 for a computational cell of $40 \times 40 \times 80$ particles. Particles are shown in a cubic cell, the volume of which is equal to the volume of a real computational cell with a non-orthogonal basis. Only particles with energies above $0.7e_{\max}$ are shown. The results were obtained for DNVM II excited with the amplitude $A = 0.04$. Panels (a–d) show the results of four numerical

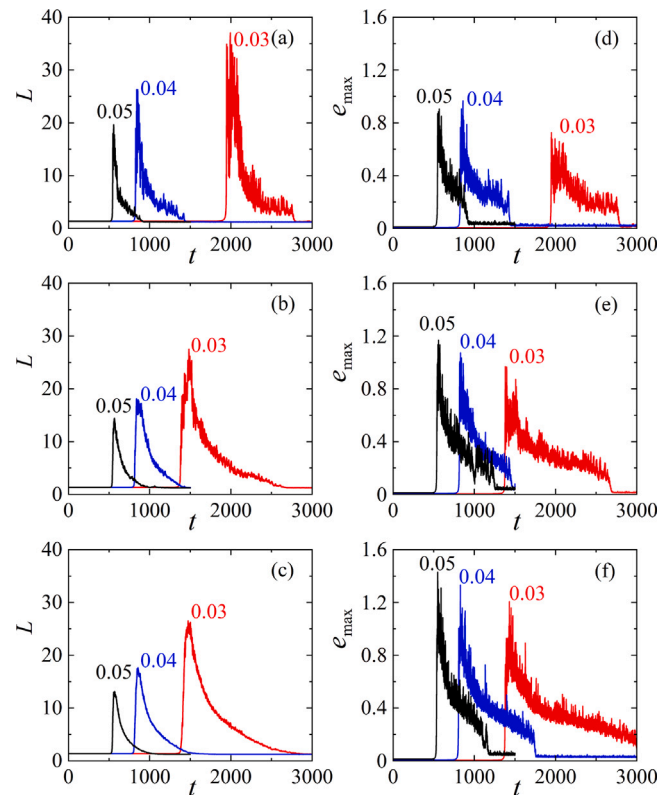


Fig. 7. (a–c) Localization parameter and (d–f) energy of the highest energy particle as the functions of time during the development of the modulational instability of DNVM III. Computational cell size: (a,d) $10 \times 10 \times 20$, (b,e) $20 \times 20 \times 40$, and (c,f) $40 \times 40 \times 80$ particles. Results for three DNVM amplitudes are presented: $A = 0.03$ red line, $A = 0.04$ blue line, and $A = 0.05$ black line. (For interpretation of the references to color in this figure legend, the reader is referred to the web version of this article.)

runs. The initial conditions were perturbed by adding to the initial displacements of particles random numbers uniformly distributed in the range $-10^{-12} \leq \rho \leq 10^{-12}$. Small initial perturbations lead to a different number of high-energy particles. Inspection of the distribution of high-energy particles over the volume of the computational cell showed that in most cases one such particle corresponds to one DB, and in rare cases DBs are presented by two neighboring high-energy particles. This means that most DBs are particle-centered and only a few are bond-centered. The numbers of DBs in Fig. 9(a–d) are 41, 38, 31 and 27, respectively. Note that Doi, Komiya, Nagashima, and Nakatani, using molecular dynamics based on embedded atom method many-body potential, have found bond-centered and particle-centered DBs in bcc vanadium [28].

Many chaotic DBs perform wandering motion, as shown in Fig. 10, where the distance of three neighboring particles from their equilibrium positions is shown as a function of time. Black, red and blue curves correspond to particles (i, j, k) , $(i, j, k+1)$, and $(i-1, j, k+1)$ respectively. At $t = t^*$, where t^* is the time when the localization parameter reaches its maximum, the particle (i, j, k) oscillates with a large amplitude. Then the oscillation amplitude of this particle begins to decrease, but its energy is spent on the excitation of the particle $(i, j, k+1)$, which then transfers its energy to the excitation of the particle $(i-1, j, k+1)$. It can be seen that the direction of energy transport changes with time. In some cases, a quasi-periodic back and forth energy exchange is observed between two neighboring particles. Partial energy exchange between DBs was observed earlier in graphene [90] and in ionic crystal with NaCl structure [91].

In Fig. 11, chaotic DBs are shown by projecting the particle trajectories onto the xy plane. In (a) and (b) the inter-site and on-site

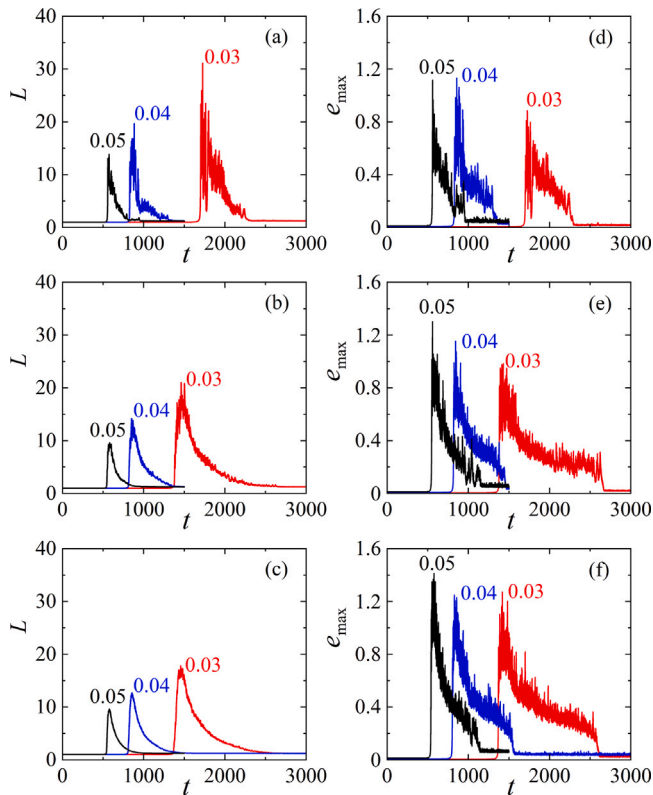


Fig. 8. (a–c) Localization parameter and (d–f) energy of the highest energy particle as the functions of time during the development of the modulational instability of DNVM IV. Computational cell size: (a,d) $10 \times 10 \times 20$, (b,e) $20 \times 20 \times 40$, and (c,f) $40 \times 40 \times 80$ particles. Results for three DNVM amplitudes are presented: $A = 0.03$ red line, $A = 0.04$ blue line, and $A = 0.05$ black line. (For interpretation of the references to color in this figure legend, the reader is referred to the web version of this article.)

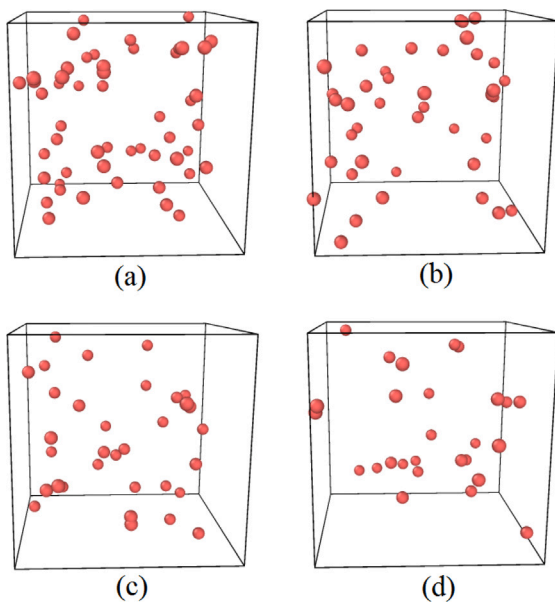


Fig. 9. High-energy particles at the time t^* of maximum localization parameter in the computational cell of $40 \times 40 \times 80$ particles. Only particles having energies greater than $0.7e_{\max}$ are shown. Initially, DNVM II was excited with amplitude $A = 0.04$ and very small random perturbations. The results of four numerical runs are shown in (a)–(d). The results differ from each other due to the stochastic nature of the chaotic DBs.

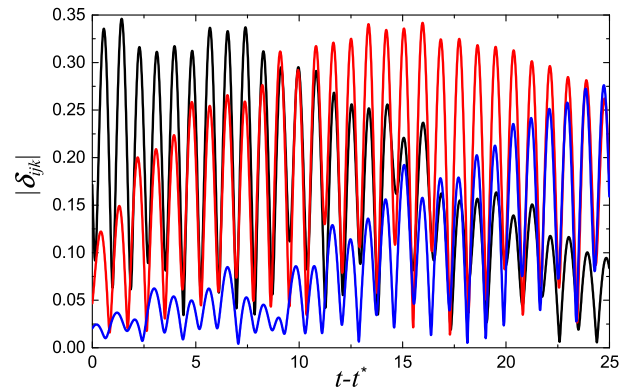


Fig. 10. Wandering motion of a chaotic DB shown by the time evolution of the distance of three neighboring particles from the equilibrium positions, $|\delta_{ijk}|$. Results for DNVM II excited with the amplitude $A = 0.04$ in the computational cell of $40 \times 40 \times 80$ particles. t^* is the time when localization parameter reaches its maximum. (For interpretation of the references to color in this figure legend, the reader is referred to the web version of this article.)

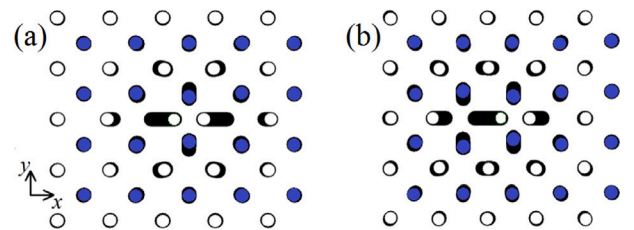


Fig. 11. Chaotic DB in (a) inter-site and (b) on-site configurations. Trajectories of particles are projected onto the xy plane. Particles belonging to two different cubic sublattices are colored white and blue. These DBs were found in the computational cell of size $40 \times 40 \times 80$ particles, where DNVM II was excited with the amplitude $A = 0.03$. (For interpretation of the references to color in this figure legend, the reader is referred to the web version of this article.)

versions of the DB are shown. While moving, the DB passes through these configurations.

6. Conclusions

In this study, we analyzed the unstable dynamics of four DNVMs with a wave vector at the boundary of the first Brillouin zone and frequencies above the phonon spectrum of the β -FPUT bcc lattice. The DNVMs were found by the group-theoretical method [69] from the analysis of the symmetry of the bcc lattice.

Development of instability of all four studied DNVMs produces chaotic DBs, if their amplitude is above a threshold value, which is of the order of magnitude of $10^{-2}h$. The appearance of DBs in the system is confirmed by the sharp increase of the energy localization parameter Eq. (18) and maximal energy of particles, see Figs. 5–8. Chaotic DBs constantly radiate energy and eventually disappear when the system reaches thermal equilibrium. During this process the energy localization parameter decreases and reaches a constant small value.

Note that in two-dimensional lattices the localization parameter decreases approximately linearly with time from its maximum value [56, 71], while in the three-dimensional bcc lattice it decreases faster, see Figs. 5–8. Such an effect of the lattice dimension on the rate of energy emission by chaotic DBs can be explained by the fact that in the 2D case the energy is emitted radially, while in the 3D lattice it is emitted spherically.

The moment of time when the localization parameter L reaches its maximum is denoted as t^* . As the DNVM amplitude increases, the rate of instability development increases and the time t^* decreases, see Figs. 5–8. On the other hand, the maximum value of L increases with

decreasing DNVM amplitude. The size of the computational cell has little effect on the dependence $L(t)$.

Chaotic DBs make a wandering motion in bcc lattice, see Fig. 10. In some cases, a quasi-periodic energy exchange between two neighboring DBs was observed, similar to what was observed for DBs in graphene [90] and in an ionic crystal with the NaCl structure [91].

In the forthcoming work, results on the modulational instability of DNVMs in a diatomic bcc lattice will be presented. DNVMs with frequencies in the bandgap will be analyzed.

CRediT authorship contribution statement

I.D. Kolesnikov: Simulations, Data curation. **S.A. Shcherbinin:** Derivation of DNVMs. **Yu.V. Bebikhov:** Simulations, Data curation. **E.A. Korznikova:** Writing revised manuscript, Response to reviewers. **I.A. Shepelev:** Discussions. **A.A. Kudreyko:** Discussions, Writing – original draft. **S.V. Dmitriev:** Conceptualization, Writing – original draft.

Declaration of competing interest

The authors declare that they have no known competing financial interests or personal relationships that could have appeared to influence the work reported in this paper.

Data availability

Data will be made available on request.

Acknowledgments

E.A.K. acknowledges the support of the Russian Science Foundation, Russia, Grant No. 21-12-00275. The contribution of A.A. Kudreyko was supported by the Bashkir State Medical University Strategic Academic Leadership Program, Russia (PRIORITY-2030).

Appendix

Let us show how the equations of motion Eq. (5) can be derived from the Hamiltonian Eq. (4).

Let the computational cell includes N particles numbered $n = 1, \dots, N$. The n th particle has the lattice position ξ_n and the displacement vector δ_n , so that its radius-vector is $r_n(t) = \xi_n + \delta_n(t)$. The Hamiltonian is the function of the particle displacements $\delta_n = (u_n, v_n, w_n)$ and velocities $\dot{\delta}_n = (\dot{u}_n, \dot{v}_n, \dot{w}_n)$,

$$H = H(\delta_n, \dot{\delta}_n) = K(\dot{\delta}_n) + P(\delta_n), \quad (20)$$

where K and P are the kinetic and potential energies of the computational cell.

According to the Hamilton's principle [92], the three equations of motion for the n th particle, in the case when $K = K(\dot{\delta}_n)$ and $P = P(\delta_n)$, are

$$\frac{d}{dt} \left(\frac{\partial K}{\partial \dot{u}_n} \right) = - \frac{\partial P}{\partial u_n}, \quad (21)$$

$$\frac{d}{dt} \left(\frac{\partial K}{\partial \dot{v}_n} \right) = - \frac{\partial P}{\partial v_n}, \quad (22)$$

$$\frac{d}{dt} \left(\frac{\partial K}{\partial \dot{w}_n} \right) = - \frac{\partial P}{\partial w_n}. \quad (23)$$

Let us derive Eq. (21) describing the motion of the n th particle along the x axis and the other two equations can be derived similarly.

The kinetic energy of the n th particle due to its motion along the x axis is $K(\dot{u}_n) = m\dot{u}_n^2/2$ and hence, the left-hand side of Eq. (21) is

$$\frac{d}{dt} \left(\frac{\partial K}{\partial \dot{u}_n} \right) = m\ddot{u}_n. \quad (24)$$

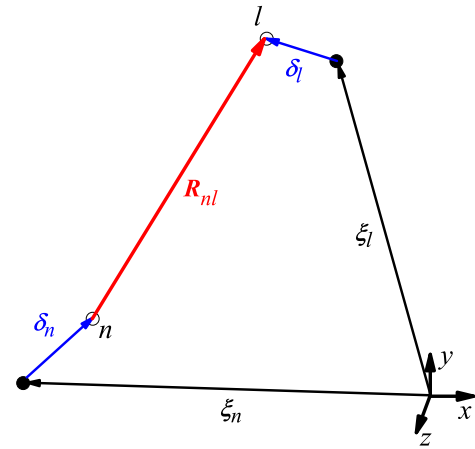


Fig. 12. Schematic representation of two interacting particles (shown by circles).

Suppose that the n th particle interacts with its L neighbors numbered $l = 1, \dots, L$. The potential energy of the computational cell P includes the L contributions that depend on the position of the n th particle,

$$P(u_n) = \sum_{l=1}^L \varphi(|\mathbf{R}_{nl}|), \quad (25)$$

where $\mathbf{R}_{nl} = (\xi_l + \delta_l) - (\xi_n + \delta_n)$ and $\varphi(|\mathbf{R}_{nl}|)$ is the potential energy of the bond connecting the n th and l th particles, see Fig. 12. The right-hand side of Eq. (21) is

$$\begin{aligned} - \frac{\partial P}{\partial u_n} &= - \sum_{l=1}^L \frac{\partial \varphi(|\mathbf{R}_{nl}|)}{\partial u_n} \\ &= - \sum_{l=1}^L \varphi'(|\mathbf{R}_{nl}|) \frac{\partial |\mathbf{R}_{nl}|}{\partial u_n} \\ &= - \sum_{l=1}^L \varphi'(|\mathbf{R}_{nl}|) \frac{R_{nl,x}}{|\mathbf{R}_{nl}|} \frac{\partial R_{nl,x}}{\partial u_n} \\ &= \sum_{l=1}^L \varphi'(|\mathbf{R}_{nl}|) \frac{R_{nl,x}}{|\mathbf{R}_{nl}|}. \end{aligned} \quad (26)$$

In the derivation of Eq. (26) it was taken into account that $R_{nl,x} = \xi_{l,x} + u_l - \xi_{n,x} - u_n$, while $R_{nl,y}$ and $R_{nl,z}$ are independent of u_n .

In view of Eqs. (24) and (26), the equation of motion of the n th particle along the x axis, Eq. (21), obtains the form

$$m\ddot{u}_n = \sum_{l=1}^L \varphi'(|\mathbf{R}_{nl}|) \frac{R_{nl,x}}{|\mathbf{R}_{nl}|}, \quad (27)$$

which essentially coincides with the first line of Eq. (5).

References

- [1] Dolgov AS. On localization of oscillations in nonlinear crystal structure. *Sov Phys—Solid State* 1986;28:907.
- [2] Sievers AJ, Takeno S. Intrinsic localized modes in anharmonic crystals. *Phys Rev Lett* 1988;61(8):970–3. <http://dx.doi.org/10.1103/PhysRevLett.61.970>.
- [3] Page JB. Asymptotic solutions for localized vibrational modes in strongly anharmonic periodic systems. *Phys Rev B* 1990;41:7835–8. <http://dx.doi.org/10.1103/PhysRevB.41.7835>.
- [4] Flach S, Willis CR. Discrete breathers. *Phys Rep* 1998;295(5):181–264. [http://dx.doi.org/10.1016/S0370-1573\(97\)00068-9](http://dx.doi.org/10.1016/S0370-1573(97)00068-9).
- [5] Campbell DK, Flach S, Kivshar YS. Localizing energy through nonlinearity and discreteness. *Phys Today* 2004;57(1):43–9. <http://dx.doi.org/10.1063/1.1650069>.
- [6] Flach S, Gorbach AV. Discrete breathers - Advances in theory and applications. *Phys Rep* 2008;467(1–3):1–116. <http://dx.doi.org/10.1016/j.physrep.2008.05.002>.

- [7] Feng B-F, Kawahara T. Discrete breathers in two-dimensional nonlinear lattices. *Wave Motion* 2007;45(1–2):68–82. <http://dx.doi.org/10.1016/j.wavemoti.2007.04.002>.
- [8] Ikeda K, Doi Y, Feng B-F, Kawahara T. Chaotic breathers of two types in a two-dimensional morse lattice with an on-site harmonic potential. *Physica D* 2007;225(2):184–96. <http://dx.doi.org/10.1016/j.physd.2006.10.017>.
- [9] Dmitriev SV, Korznikova EA, Baimova JA, Velarde MG. Discrete breathers in crystals. *Phys-Usp* 2016;59(5):446–61. <http://dx.doi.org/10.3367/UFNr.2016.02.037729>.
- [10] Manley ME, Yethiraj M, Sinn H, Volz HM, Alatas A, Lashley JC, Hulst WL, Lander GH, Smith JL. Formation of a new dynamical mode in α -uranium observed by inelastic X-Ray and neutron scattering. *Phys Rev Lett* 2006;96:125501. <http://dx.doi.org/10.1103/PhysRevLett.96.125501>.
- [11] Manley ME, Lynn JW, Chen Y, Lander GH. Intrinsically localized mode in α -U as a precursor to a solid-state phase transition. *Phys Rev B* 2008;77:052301. <http://dx.doi.org/10.1103/PhysRevB.77.052301>.
- [12] Manley ME, Sievers AJ, Lynn JW, Kiselev SA, Agladze NI, Chen Y, Llobet A, Alatas A. Intrinsic localized modes observed in the high-temperature vibrational spectrum of NaI. *Phys Rev B* 2009;79:134304. <http://dx.doi.org/10.1103/PhysRevB.79.134304>.
- [13] Sievers AJ, Sato M, Page JB, Rössler T. Thermally populated intrinsic localized modes in pure alkali halide crystals. *Phys Rev B* 2013;88:104305. <http://dx.doi.org/10.1103/PhysRevB.88.104305>, URL <http://link.aps.org/doi/10.1103/PhysRevB.88.104305>.
- [14] Kiselev SA, Sievers AJ. Generation of intrinsic vibrational gap modes in three-dimensional ionic crystals. *Phys Rev B* 1997;55:5755–8. <http://dx.doi.org/10.1103/PhysRevB.55.5755>, URL <http://link.aps.org/doi/10.1103/PhysRevB.55.5755>.
- [15] Khadeeva LZ, Dmitriev SV. Discrete breathers in crystals with NaCl structure. *Phys Rev B* 2010;81:214306. <http://dx.doi.org/10.1103/PhysRevB.81.214306>, URL <http://link.aps.org/doi/10.1103/PhysRevB.81.214306>.
- [16] Rivière A, Lepri S, Colognesi D, Piazza F. Wavelet imaging of transient energy localization in nonlinear systems at thermal equilibrium: The case study of NaI crystals at high temperature. *Phys Rev B* 2019;99:024307. <http://dx.doi.org/10.1103/PhysRevB.99.024307>.
- [17] Voulgarakis NK, Hadjisavvas G, Kelires PC, Tsironis GP. Computational investigation of intrinsic localization in crystalline Si. *Phys Rev B* 2004;69:113201. <http://dx.doi.org/10.1103/PhysRevB.69.113201>.
- [18] Murzaev RT, Bachurin DV, Korznikova EA, Dmitriev SV. Localized vibrational modes in diamond. *Phys Lett A* 2017;381(11):1003–8. <http://dx.doi.org/10.1016/j.physleta.2017.01.014>.
- [19] Haas M, Hizhnyakov V, Shelkan A, Klopov M, Sievers AJ. Prediction of high-frequency intrinsic localized modes in Ni and Nb. *Phys Rev B* 2011;84:144303. <http://dx.doi.org/10.1103/PhysRevB.84.144303>, URL <http://link.aps.org/doi/10.1103/PhysRevB.84.144303>.
- [20] Morkina AY, Bachurin DV, Dmitriev SV, Semenov AS, Korznikova EA. Modulational instability of delocalized modes in fcc copper. *Materials* 2022;15(16):5597. <http://dx.doi.org/10.3390/ma15165597>.
- [21] Bachurina OV, Kudreyko AA. Two-dimensional discrete breathers in fcc metals. *Comput Mater Sci* 2020;182:109737. <http://dx.doi.org/10.1016/j.commatsci.2020.109737>.
- [22] Bachurina OV, Murzaev RT, Bachurin DV. Molecular dynamics study of two-dimensional discrete breather in nickel. *J Micromech Mol Phys* 2019;4(2):1950001. <http://dx.doi.org/10.1142/S2424913019500012>.
- [23] Bachurina OV. Plane and plane-radial discrete breathers in fcc metals. *Model Simul Mater Sci* 2019;27(5):055001. <http://dx.doi.org/10.1088/1361-651X/ab17b7>.
- [24] Bachurina OV. Linear discrete breather in fcc metals. *Comput Mater Sci* 2019;160:217–21. <http://dx.doi.org/10.1016/j.commatsci.2019.01.014>.
- [25] Bachurina OV, Kudreyko AA. Two-component localized vibrational modes in fcc metals. *Eur Phys J B* 2021;94(11):218. <http://dx.doi.org/10.1140/epjb/s10051-021-00227-3>.
- [26] Krylova KA, Lobzenko IP, Semenov AS, Kudreyko AA, Dmitriev SV. Spherically localized discrete breathers in bcc metals V and Nb. *Comput Mater Sci* 2020;180:109695. <http://dx.doi.org/10.1016/j.commatsci.2020.109695>.
- [27] Murzaev RT, Kistanov AA, Dubinko VI, Terentyev DA, Dmitriev SV. Moving discrete breathers in bcc metals V, Fe and W. *Comput Mater Sci* 2015;98:88–92. <http://dx.doi.org/10.1016/j.commatsci.2014.10.061>.
- [28] Doi Y, Komiya T, Nagashima S, Nakatani A. Search of nonlinear energy localized structure in bcc crystals. *Zairyo/J Soc Mater Sci Japan* 2021;70(4):330–5. <http://dx.doi.org/10.2472/jms.70.330>.
- [29] Bachurina OV, Murzaev RT, Kudreyko AA, Dmitriev SV, Bachurin DV. Atomistic study of two-dimensional discrete breathers in hcp titanium. *Eur Phys J B* 2022;95(7):104. <http://dx.doi.org/10.1140/epjb/s10051-022-00367-0>.
- [30] Bachurina OV, Murzaev RT, Semenov AS, Korznikova EA, Dmitriev SV. Properties of moving discrete breathers in beryllium. *Phys Solid State* 2018;60(5):989–94. <http://dx.doi.org/10.1134/S1063783418050049>.
- [31] Murzaev RT, Babicheva RI, Zhou K, Korznikova EA, Fomin SY, Dubinko VI, Dmitriev SV. Discrete breathers in alpha-uranium. *Eur Phys J B* 2016;89(7):168. <http://dx.doi.org/10.1140/epjb/e2016-70142-3>.
- [32] Medvedev NN, Starostenkov MD, Manley ME. Energy localization on the Al sublattice of Pt₃Al with L1₂ order. *J Appl Phys* 2013;114(21):213506. <http://dx.doi.org/10.1063/1.4837598>.
- [33] Medvedev NN, Starostenkov MD, Zakharov PV, Pozidaeva OV. Localized oscillating modes in two-dimensional model of regulated Pt₃Al alloy. *Tech Phys Lett* 2011;37(2):98–101. <http://dx.doi.org/10.1134/S1063785011020106>.
- [34] Zakharov PV, Korznikova EA, Dmitriev SV, Komarov EG, Zhou K. Surface discrete breathers in Pt₃Al intermetallic alloy. *Surf Sci* 2019;679:1–5. <http://dx.doi.org/10.1016/j.susc.2018.08.011>.
- [35] Khadeeva LZ, Dmitriev SV. Lifetime of gap discrete breathers in diatomic crystals at thermal equilibrium. *Phys Rev B* 2011;84:144304. <http://dx.doi.org/10.1103/PhysRevB.84.144304>.
- [36] Korznikova EA, Fomin SY, Soboleva EG, Dmitriev SV. Highly symmetric discrete breather in a two-dimensional morse crystal. *JETP Lett* 2016;103(4):277–81. <http://dx.doi.org/10.1134/S0021364016040081>.
- [37] Savin AV, Dmitriev SV. Influence of the internal degrees of freedom of coronene molecules on the nonlinear dynamics of a columnar chain. *Phys Rev E* 2023;107:054216. <http://dx.doi.org/10.1103/PhysRevE.107.054216>.
- [38] Savin AV, Korznikova EA, Dmitriev SV. Plane vibrational modes and localized nonlinear excitations in carbon nanotube bundle. *J Sound Vib* 2022;520:116627. <http://dx.doi.org/10.1016/j.jsv.2021.116627>.
- [39] Kinoshita Y, Yamayose Y, Doi Y, Nakatani A, Kitamura T. Selective excitations of intrinsic localized modes of atomic scales in carbon nanotubes. *Phys Rev B* 2008;77:024307. <http://dx.doi.org/10.1103/PhysRevB.77.024307>.
- [40] Shimada T, Shirasaki D, Kitamura T. Stone-Wales transformations triggered by intrinsic localized modes in carbon nanotubes. *Phys Rev B* 2010;81:035401. <http://dx.doi.org/10.1103/PhysRevB.81.035401>.
- [41] Shimada T, Shirasaki D, Kinoshita Y, Doi Y, Nakatani A, Kitamura T. Influence of nonlinear atomic interaction on excitation of intrinsic localized modes in carbon nanotubes. *Physica D* 2010;239:407–13. <http://dx.doi.org/10.1016/j.physd.2010.01.001>.
- [42] Onyibo EC, Safaei B. Application of finite element analysis to honeycomb sandwich structures: a review. *Rep Mech Eng* 2022;3(1):192–209. <http://dx.doi.org/10.31181/rme200230320220>.
- [43] Yamayose Y, Kinoshita Y, Doi Y, Nakatani A, Kitamura T. Excitation of intrinsic localized modes in a graphene sheet. *Europhys Lett* 2007;80:40008. <http://dx.doi.org/10.1209/0295-5075/80/40008>.
- [44] Hizhnyakov V, Klopov M, Shelkan A. Transverse intrinsic localized modes in monatomic chain and in graphene. *Phys Lett A* 2016;380(9–10):1075–81. <http://dx.doi.org/10.1016/j.physleta.2016.01.011>.
- [45] Fraile A, Koukaras E, Papagelis K, Lazarides N, Tsironis G. Long-lived discrete breathers in free-standing graphene. *Chaos Solitons Fractals* 2016;87:262–7. <http://dx.doi.org/10.1016/j.chaos.2016.04.015>.
- [46] Doi Y, Nakatani A. Structure and stability of nonlinear vibration mode in graphene sheet. *Procedia Eng* 2011;10:3393–8. <http://dx.doi.org/10.1016/j.proeng.2011.04.559>.
- [47] Chechin GM, Dmitriev SV, Lobzenko IP, Ryabov DS. Properties of discrete breathers in graphane from *ab initio* simulations. *Phys Rev B* 2014;90:045432. <http://dx.doi.org/10.1103/PhysRevB.90.045432>.
- [48] Krylova KA, Baimova JA, Murzaev RT, Mulyukov RR. Energy exchange between discrete breathers in graphane in the mutual equilibrium. *Phys Lett Sect A: Gen Atom Solid State Phys* 2019;383(14):1583–8. <http://dx.doi.org/10.1016/j.physleta.2019.02.033>.
- [49] Cuevas J, Archilla JFR, Sánchez-Rey B, Romero F. Interaction of moving discrete breathers with vacancies. *Physica D* 2006;216(1 SPEC. ISS.):115–20. <http://dx.doi.org/10.1016/j.physd.2005.12.022>.
- [50] Terentyev DA, Dubinko AV, Dubinko VI, Dmitriev SV, Zhurkin EE, Sorokin MV. Interaction of discrete breathers with primary lattice defects in bcc Fe. *Modelling Simul Mater Sci Eng* 2015;23(8):085007. <http://dx.doi.org/10.1088/0965-0393/23/8/085007>.
- [51] Abdullina DU, Bebikhov YV, Khazimullin MV, Kudreyko AA, Dmitriev SV. Atom deposition and sputtering at normal incidence simulated by the Frenkel-Kontorova chain. *Phys Rev E* 2022;106(2):024207. <http://dx.doi.org/10.1103/PhysRevE.106.024207>.
- [52] Moradi Marjaneh A, Saadatmand D, Evazzade I, Babicheva RI, Soboleva EG, Srikanth N, Zhou K, Korznikova EA, Dmitriev SV. Mass transfer in the Frenkel-Kontorova chain initiated by molecule impact. *Phys Rev E* 2018;98(2):023003. <http://dx.doi.org/10.1103/PhysRevE.98.023003>.
- [53] Manley ME. Impact of intrinsic localized modes of atomic motion on materials properties. *Acta Mater* 2010;58(8):2926–35. <http://dx.doi.org/10.1016/j.actamat.2010.01.021>.
- [54] Dubinko VI, Selyshchev PA, Archilla JFR. Reaction-rate theory with account of the crystal anharmonicity. *Phys Rev E* 2011;83:041124. <http://dx.doi.org/10.1103/PhysRevE.83.041124>.
- [55] Korznikova EA, Morkina AY, Singh M, Krivtsov AM, Kuzkin VA, Gani VA, Bebikhov YV, Dmitriev SV. Effect of discrete breathers on macroscopic properties of the Fermi-Pasta-Ulam chain. *Eur Phys J B* 2020;93(7):123. <http://dx.doi.org/10.1140/epjb/e2020-10173-7>.

- [56] Upadhyaya A, Semenova MN, Kudreyko AA, Dmitriev SV. Chaotic discrete breathers and their effect on macroscopic properties of triangular lattice. *Commun Nonlinear Sci* 2022;112:106541. <http://dx.doi.org/10.1016/j.cnsns.2022.106541>.
- [57] Singh M, Morkina AY, Korznikova EA, Dubinko VI, Terentiev DA, Xiong D, Naimark OB, Gani VA, Dmitriev SV. Effect of discrete breathers on the specific heat of a nonlinear chain. *J Nonlinear Sci* 2021;31(1):12. <http://dx.doi.org/10.1007/s00332-020-09663-4>.
- [58] Baimova JA, Murzaev RT, Rudskoy AI. Discrete breathers in graphane in thermal equilibrium. *Phys Lett Sect A: Gen Atom Solid State Phys* 2017;381(36):3049–53. <http://dx.doi.org/10.1016/j.physleta.2017.07.027>.
- [59] Burlakov VM, Kiselev SA, Rupasov VI. Localized vibrations of homogeneous anharmonic chains. *Phys Lett A* 1990;147(2):130–4. [http://dx.doi.org/10.1016/0375-9601\(90\)90880-W](http://dx.doi.org/10.1016/0375-9601(90)90880-W).
- [60] Dauxois T, Khermeriki R, Piazza F, Ruffo S. The anti-FPU problem. *Chaos* 2005;15(1):015110. <http://dx.doi.org/10.1063/1.1854273>.
- [61] Daumont I, Dauxois T, Peyrard M. Modulational instability: First step towards energy localization in nonlinear lattices. *Nonlinearity* 1997;10(3):617–30. <http://dx.doi.org/10.1088/0951-7715/10/3/003>.
- [62] Yoshimura K. Modulational instability of zone boundary mode in nonlinear lattices: Rigorous results. *Phys Rev E* 2004;70(1 2):016611. <http://dx.doi.org/10.1103/PhysRevE.70.016611>.
- [63] Kosevich YA, Lepri S. Modulational instability and energy localization in anharmonic lattices at finite energy density. *Phys Rev B* 2000;61(1):299–307. <http://dx.doi.org/10.1103/PhysRevB.61.299>.
- [64] Tang B, Deng K. Discrete breathers and modulational instability in a discrete ϕ^4 nonlinear lattice with next-nearest-neighbor couplings. *Nonlinear Dynam* 2017;88(4):2417–26. <http://dx.doi.org/10.1007/s11071-017-3386-4>.
- [65] Kavitha L, Mohamadou A, Parasuraman E, Gopi D, Akila N, Prabhu A. Modulational instability and nano-scale energy localization in ferromagnetic spin chain with higher order dispersive interactions. *J Magn Magn Mater* 2016;404:91–118. <http://dx.doi.org/10.1016/j.jmmm.2015.11.036>.
- [66] Kavitha L, Parasuraman E, Gopi D, Prabhu A, Vicencio RA. Nonlinear nano-scale localized breather modes in a discrete weak ferromagnetic spin lattice. *J Magn Magn Mater* 2016;401:394–405. <http://dx.doi.org/10.1016/j.jmmm.2015.10.021>.
- [67] Korznikova EA, Bachurin DV, Fomin SY, Chetverikov AP, Dmitriev SV. Instability of vibrational modes in hexagonal lattice. *Eur Phys J B* 2017;90(2):23. <http://dx.doi.org/10.1140/epjb/e2016-70595-2>.
- [68] Babicheva RI, Semenov AS, Soboleva EG, Kudreyko AA, Zhou K, Dmitriev SV. Discrete breathers in a triangular β -Fermi-Pasta-Ulam-tsingou lattice. *Phys Rev E* 2021;103:052202. <http://dx.doi.org/10.1103/PhysRevE.103.052202>.
- [69] Chechin GM, Sakhnenko VP. Interactions between normal modes in nonlinear dynamical systems with discrete symmetry. Exact results. *Physica D* 1998;117(1–4):43–76. [http://dx.doi.org/10.1016/S0167-2789\(98\)80012-2](http://dx.doi.org/10.1016/S0167-2789(98)80012-2).
- [70] Ryabov DS, Chechin GM, Upadhyaya A, Korznikova EA, Dubinko VI, Dmitriev SV. Delocalized nonlinear vibrational modes of triangular lattices. *Nonlinear Dynam* 2020;102(4):2793–810. <http://dx.doi.org/10.1007/s11071-020-06015-5>.
- [71] Ryabov DS, Chechin GM, Naumov EK, Bebiukhov YV, Korznikova EA, Dmitriev SV. One-component delocalized nonlinear vibrational modes of square lattices. *Nonlinear Dynam* 2023;111(9):8135–53. <http://dx.doi.org/10.1007/s11071-023-08264-6>.
- [72] Naumov E, Bebiukhov Y, Ekomasov E, Soboleva E, Dmitriev S. Discrete breathers in square lattices from delocalized nonlinear vibrational modes. *Phys Rev E* 2023;107(3):034214. <http://dx.doi.org/10.1103/PhysRevE.107.034214>.
- [73] Babicheva RI, Semenov AS, Shcherbinin SA, Korznikova EA, Kudreyko AA, Vivegananthan P, Zhou K, Dmitriev SV. Effect of the stiffness of interparticle bonds on properties of delocalized nonlinear vibrational modes in an fcc lattice. *Phys Rev E* 2022;105(5):064204. <http://dx.doi.org/10.1103/PhysRevE.105.064204>.
- [74] Kosarev IV, Shcherbinin SA, Kistanov AA, Babicheva RI, Korznikova EA, Dmitriev SV. An approach to evaluate the accuracy of interatomic potentials as applied to tungsten. *Comput Mater Sci* 2024;231:112597. <http://dx.doi.org/10.1016/j.commatsci.2023.112597>.
- [75] Chechin G, Ryabov D, Shcherbinin S. Nonlinear normal mode interactions in the SF₆ molecule studied with the aid of density functional theory. *Phys Rev E* 2015;92(1):012907. <http://dx.doi.org/10.1103/PhysRevE.92.012907>.
- [76] Chechin GM, Novikova NV, Abramenko AA. Bushes of vibrational modes for Fermi-Pasta-Ulam chains. *Physica D* 2002;166(3–4):208–38. [http://dx.doi.org/10.1016/S0167-2789\(02\)00430-X](http://dx.doi.org/10.1016/S0167-2789(02)00430-X).
- [77] Chechin GM, Ryabov DS, Shcherbinin SA. Nonlinear vibrational modes in graphene: Group-theoretical results. *Lett Mater* 2016;6(1):9–15. <http://dx.doi.org/10.22226/2410-3535-2016-1-9-15>, cited By 25.
- [78] Chechin G, Ryabov D, Shcherbinin S. Large-amplitude periodic atomic vibrations in diamond. *J Micromech Mol Phys* 2018;3(1–2):1850002. <http://dx.doi.org/10.1142/S2424913018500029>.
- [79] Chechin G, Ryabov D. Exact solutions of nonlinear dynamical equations for large-amplitude atomic vibrations in arbitrary monoatomic chains with fixed ends. *Commun Nonlinear Sci* 2023;120:107176. <http://dx.doi.org/10.1016/j.cnsns.2023.107176>.
- [80] Shcherbinin SA, Krylova KA, Chechin GM, Soboleva EG, Dmitriev SV. Delocalized nonlinear vibrational modes in fcc metals. *Commun Nonlinear Sci Numer Simul* 2022;104:106039. <http://dx.doi.org/10.1016/j.cnsns.2021.106039>.
- [81] Zhang Y, Li K, Zhao H. Intense terahertz radiation: generation and application. *Front Optoelectron* 2021;14(1):4–36. <http://dx.doi.org/10.1007/s12200-020-1052-9>.
- [82] Zhang XC, Shkurinov A, Zhang Y. Extreme terahertz science. *Nat Photonics* 2017;11(1):16–8. <http://dx.doi.org/10.1038/nphoton.2016.249>.
- [83] Liao G, Li Y, Liu H, Scott GG, Neely D, Zhang Y, Zhu B, Zhang Z, Armstrong C, Zemaityte E, Bradford P, Huggard PG, Rusby DR, McKenna P, Brenner CM, Woolsey NC, Wang W, Sheng Z, Zhang J. Multimillijoule coherent terahertz bursts from picosecond laser-irradiated metal foils. *Proc Natl Acad Sci USA* 2019;116(10):3994–9. <http://dx.doi.org/10.1073/pnas.1815256116>.
- [84] Nicoletti D, Cavalleri A. Nonlinear light–matter interaction at terahertz frequencies. *Adv Opt Photonics* 2016;8(3):401–64. <http://dx.doi.org/10.1364/AOP.8.000401>.
- [85] Hafez HA, Chai X, Ibrahim A, Mondal S, Férachou D, Ropagnol X, Ozaki T. Intense terahertz radiation and their applications. *J Opt UK* 2016;18(9):093004. <http://dx.doi.org/10.1088/2040-8978/18/9/093004>.
- [86] Leitenstorfer A, Moskalenko AS, Kampfrath T, Kono J, Castro-Camus E, Peng K, Qureshi N, Turchinovich D, Tanaka K, Markelz A, Havenith M, Hough C, Joyce HJ, Padilla WJ, Zhou B, Kim K-Y, Zhang X-C, Jepsen PU, Dhillon S, Vitiello M, Linfield E, Davies AG, Hoffmann MC, Lewis R, Tonouchi M, Klarskov P, Seifert TS, Gerasimenko Y, Mihailovic D, Huber R, Boland JL, Mitrofanov O, Dean P, Ellison B, Huggard P, Rea S, Walker C, Leisawitz DT, Gao J, Li C, Chen Q, Valušis G, Wallace VP, Pickwell-MacPherson E, Shang X, Hesler J, Ridler N, Renaud CC, Kallfass I, Nagatsuma T, Zeitler JA, Arnone D, Johnston MB, Cunningham J. The 2023 terahertz science and technology roadmap. *J Phys D: Appl Phys* 2023;56(22). <http://dx.doi.org/10.1088/1361-6463/acbe4c>.
- [87] Bakhvalov NS. Numerical methods: Analysis, algebra, ordinary differential equations. Moscow: MIR Publishers; 1977.
- [88] Stearrett R, English LQ. Experimental generation of intrinsic localized modes in a discrete electrical transmission line. *J Phys D: Appl Phys* 2007;40(17):5394–8. <http://dx.doi.org/10.1088/0022-3727/40/17/058>.
- [89] Abdullina DU, Semenova MN, Semenov AS, Korznikova EA, Dmitriev SV. Stability of delocalized nonlinear vibrational modes in graphene lattice. *Eur Phys J B* 2019;92(11):249. <http://dx.doi.org/10.1140/epjb/e2019-100436-y>.
- [90] Baimova JA, Dmitriev SV, Zhou K. Discrete breather clusters in strained graphene. *Europhys Lett* 2012;100(3):36005. <http://dx.doi.org/10.1209/0295-5075/100/36005>.
- [91] Kistanov AA, Dmitriev SV. Energy exchange between discrete breathers in crystal with NaCl structure. *Tech Phys Lett* 2013;39(7):618–20. <http://dx.doi.org/10.1134/S1063785013070079>.
- [92] Landau LD, Lifshitz EM. *Mechanics*. Pergamon Press; 1976.